Rock Mech Rock Eng
DOI 10.1007/s00603-016-1126-6

ORIGINAL PAPER

On the Variable Dilatancy Angle in Rocks Around Underground Galleries

Fatemeh Salehnia[1] · **Frédéric Collin**[1] · **Robert Charlier**[1]

Received: 6 February 2016 / Accepted: 22 October 2016

Abstract Correct estimation of the dilatant behavior of a rock has an essential role in a realistic numerical simulation of the fracturing threshold during the rock deformation process and its post-failure response, based on experimental and field observations. This importance has been poorly treated in most of the numerical analyses dealing with the rock engineering common problems such as deep excavations. The dilatancy angle as a commonly used parameter for describing the dilatation response of a rock is mostly simplified to be a constant value. Contrarily, a literature review declares the inadequacy of this approach in those rock mechanics applications. In the present paper, a new formula for considering the variable dilatancy angle is presented which relates this parameter to the plastic shear strain in the course of a loading procedure. It is aimed at characterizing an evolution of the dilatant or contracting volumetric response of a rock as well as giving the possibility to simulate a dilatant/contracting transitional behavior. The model is applied to simulate the development of strain localization, in shear band mode, within the inevitable excavation damaged zone created around an underground opening in rock. It is illustrated that using the model of variable dilatancy angle in a deep excavation modeling could help to better reproduce the fractures development around the opening in the course of tunneling.

Keywords Dilatancy angle · Plastic strain · Gallery excavation · Strain localization · Pore water pressure

✉ Fatemeh Salehnia
f.salehnia@alumni.ulg.ac.be

[1] Département ArGEnCo, Universitè de Liège, Allée de la Découverte 9, 4000 Liège, Belgium

List of symbols

Roman symbols

B_φ, B_c, B_Ψ	The value of equivalent plastic strain from which hardening/softening on friction angle/cohesion, and the change in dilatancy angle is started
c_i, c_f	Initial and final cohesions
D	Second gradient elastic modulus
D_φ, D_c, D_Ψ	The value of equivalent plastic strain for which half of the hardening/softening on friction angle/cohesion, and the change in dilatancy angle is achieved
E	Young's modulus
F_{ij}	Macrodeformation gradient field
$F^\star_{ij}$	Kinematically admissible macrodeformation gradient field
g	Potential surface
$h^\star_{ijk}$	Virtual microsecond gradient field
I_σ	First stress tensor invariant
$II_{\hat{\sigma}}$	Second deviatoric stress tensor invariant
k_w	Intrinsic permeability
$K^\star_p$	Tangent dilatancy factor
m_i	Water mass flow
n	Porosity
p_w	Pore water pressure field
$p^\star_w$	Kinematically admissible virtual pore water pressure field
$\overline{q}$	Prescribed water mass per unit area
Q	Water sink term
Rat_Ψ	Ratio between the peak of dilatancy angle and its initial value
$\dot{S}$	Time derivative of water mass
t	Time

Published online: 11 November 2016

$\bar{t}_i$	Classical external traction force per unit area
$\overline{T}_i$	Additional external double surface force per unit area
u_i	Displacement vector
$u_i^{\star}$	Kinematically admissible virtual displacement vector
$\mathscr{W}_{\mathrm{I}}^{\star}, \mathscr{W}_{\mathrm{E}}^{\star}$	Internal and external virtual work

Greek symbols

Γ	Plastic shear strain
δ_{ij}	Kronecker delta
$\Delta^{\star}$	Maximum inelastic volume increase
ε_{ij}	Strain tensor
$\dot{\varepsilon}_1^{\mathrm{p}}, \dot{\varepsilon}_3^{\mathrm{p}}$	Major and minor principle plastic strain increment
$\dot{\varepsilon}_{ij}^{\mathrm{p}}$	Plastic component of strain tensor rate
$\dot{\varepsilon}_{\mathrm{v}}^{\mathrm{p}}$	Volumetric plastic strain increment
$\varepsilon_{\mathrm{eq}}^{\mathrm{p}}$	Von Mises equivalent plastic strain
$\dot{\varepsilon}_{\mathrm{eq}}^{\mathrm{p}}$	Von Mises equivalent plastic strain rate
$\dot{\lambda}$	Plastic multiplier
λ_{ij}	Field of Lagrange multipliers
μ_{w}	Water dynamic viscosity
ν	Poisson ratio
ρ_{s}	Specific mass of the grains
ρ_{w}	Specific mass of the water
σ_{ij}	Total stress tensor
σ'_{ij}	Effective stress tensor
$\hat{\sigma}'_{ij}$	Deviatoric stress tensor
Σ_{ijk}	Double stress
τ_{ij}	Microstress tensor
υ_{ij}	Microkinematic gradient field
$\upsilon_{ij}^{\star}$	Virtual microkinematic gradient field
$\varphi_{\mathrm{c0}}, \varphi_{\mathrm{cf}}$	Initial and final compression friction angles
φ_{cv}	Friction angle at constant volume
$1/\chi_{\mathrm{w}}$	Water compressibility
Ψ	Dilatancy angle
Ψ_{peak}	Peak value of dilatancy angle
Ψ_{lim}	Limit value of dilatancy angle
Ω	Current solid configuration

1 Introduction

A short review of the literature regarding the experimental and field observations of the soils and rocks behavior evidences how important is addressing their correct volumetric response in the process of a realistic numerical analysis of their coupled hydro-mechanical behavior. The rock failure and post-failure processes are in fact frequently associated to its dilatation. Nevertheless, this issue has received very little attention in rock engineering.

To describe the dilatant behavior of a material, dilatancy angle, Ψ, is a suitable parameter (Vermeer and De Borst 1984) that is widely used. Indeed, this parameter has not been frequently taken into account in the numerical studies in rock mechanics or while it has been considered, the used approach has not been often well developed. Some of the researchers used the simplistic methods taking into account a constant dilatancy angle, according to Detournay (1986) and Alejano and Alonso (2005); it mostly consisted in considering a zero value for a non-associated flow rule and equal to friction angle for an associated flow rule. Although, considering an associated flow rule does not undoubtedly reproduce properly the post-failure response of a rock (Vermeer and De Borst 1984). The influence of non-associativity has been particularly studied in Zervos et al. (2007). Furthermore, the introduced value of dilatancy angle must not be realistically constant—when a material is deformed—in order to be able to address the correct hydro-mechanical response of the material during a gradual loading process. The need to consider the variable dilatancy was primitively concluded by Detournay (1986). This author has indicated that the assumption of a constant dilatancy angle is believed to be unrealistic proposing that the dilatancy of a rock is a function of the plastic shear strain. This need has been subsequently more illustrated in some other similar studies which have considered the variable dilation (e.g., see Papanastasiou and Vardoulakis 1992; Alejano and Alonso 2005; Papamichos 2010).

Considering the numerical simulation of a triaxial compression test, as a frequently used test in soil and rock mechanics for characterizing the stress–strain curve of a material and its volumetric response, correct estimation of dilatancy angle could be influential. Introduction of a dilatancy angle into a numerical model could directly influence the obtained volumetric response of a material in the simulation of a drained triaxial test, and it might change the obtained pore pressure evolution in an undrained triaxial test (Salehnia 2015). The latter affects also the strengthening mechanism and failure process of the material with respect to a coupled hydro-mechanical analysis. In the larger scale, correct evaluation of dilatancy is of significant importance in analyzing the fracture development, extension of damaged zone and fluid flow behavior in rocks around the underground excavations. Indeed, considering a constant dilatancy angle in simulating the above phenomena is not physically realistic. This latter large-scale application of practical interest in rock engineering is focused in this paper.

Thence, to estimate more realistically the dilatancy angle and its variations, further research and development is of paramount interest. This paper proposes a new formula for considering the variable dilatancy angle incorporated into the framework of an elasto-plastic

hardening/softening model. The proposed formula for estimating the change in dilatancy angle has been developed in a semi-empirical manner with respect to an analysis of a clay rock response during the triaxial tests and tunnel excavation. However, it can be reliably supposed to address the volumetric behavior of any rock and clay stones. The new proposition has been intended to be able to characterize an evolution of the dilatant, contracting, dilatant/contracting transitional responses of a material following its loading procedure.

In the following, subsequently to the dilatancy angle definition in the literature point of view, the new proposition is formulated within the classical used theoretical framework. The model is then validated through the numerical simulation of a deep gallery excavation. This refers to tunneling through the stable geological Boom clay formation, located in north of Belgium, within the framework of studying the feasibility of deep storage of high-level radioactive waste in this formation. Boom clay is a plastic clay, which has been selected as a reference host formation in Belgium for deep disposal of high-level radioactive waste (ONDRAF/NIRAS 2001). It is then supposed to play the most essential role as a natural barrier (Chapman and Hooper 2012) that ensures adequate isolation of radionuclides from man and environment, besides the engineered barriers. To correctly characterize the response of this material in the framework of a natural barrier, numerous research activities and experimental works have been organized (Bastiaens et al. 2003; Coll 2005; Bernier et al. 2007b; Bésuelle et al. 2014). With reference to those, some numerical works have been aimed at reproducing realistically the material's behavior (Salehnia et al. 2015a, b; Salehnia 2015).

In the course of a gallery excavation, important stress redistribution within a perturbed zone is expected around the underground opening. It can consequently trigger the macro and microfracturing and lead to the creation of a zone, called Excavation Damaged Zone (EDZ), with significant irreversible deformations and changes of hydro-mechanical host rock's properties (Tsang et al. 2005; Blümling et al. 2007). The shear induced fractures have been frequently observed within this zone in clay formations and they were also evidenced during the excavations in Boom clay host rock (Mertens et al. 2004; Blümling et al. 2007). In addition, these shear zones are frequently preceded by development of the localization of strains in narrow so-called shear bands. Therefore, the EDZ is proposed to be realistically analyzed by numerical simulation using a strain localization approach in shear bands mode (e.g., see Salehnia et al. 2015b; Charlier et al. 2015). Within this framework, a realistic evaluation of dilatancy is of significant importance in analyzing the fracturing threshold during the rock deformation process and post-failure mechanisms. It could then help to a better simulation of the fractures development within the EDZ around the gallery.

2 Overview of the Dilatancy Angle Interest and Encountered Difficulty

Dilatancy may be defined as an inelastic change in volume that is associated to shear distortion of an element in the material (Vermeer and De Borst 1984). The dilatancy parameter (commonly used dilatancy angle) is important for characterizing the soil and rock behavior when they are deformed.

Vermeer and De Borst (1984) proposed an estimation of the dilatancy angle for rocks, granular soils and concrete as follows:

$$\Psi = \arcsin\frac{\dot{\varepsilon}_{\mathrm{v}}^{\mathrm{p}}}{-2\dot{\varepsilon}_{1}^{\mathrm{p}} + \dot{\varepsilon}_{\mathrm{v}}^{\mathrm{p}}} \quad \text{for } \sigma_1 < \sigma_2 \leq \sigma_3 \tag{1}$$

where $\dot{\varepsilon}_{\mathrm{v}}^{\mathrm{p}}$ is the volumetric plastic strain increment, $\dot{\varepsilon}_{1}^{\mathrm{p}}$ is the major (axial) plastic strain increment. The advantage of this formula to the classical notation used for a non-hardening model (Eq. 2), as the authors indicated, is that Eq. 1 is also valid for a common triaxial compression case ($\sigma_1 < \sigma_2 = \sigma_3$).

$$\Psi = \arcsin\frac{\dot{\varepsilon}_{1}^{\mathrm{p}} + \dot{\varepsilon}_{3}^{\mathrm{p}}}{-\dot{\varepsilon}_{1}^{\mathrm{p}} + \dot{\varepsilon}_{3}^{\mathrm{p}}} \quad \text{for } \sigma_1 < \sigma_2 < \sigma_3 \tag{2}$$

where $\dot{\varepsilon}_{1}^{\mathrm{p}}$ and $\dot{\varepsilon}_{3}^{\mathrm{p}}$ are major and minor principle plastic strains. Based on the analysis of these authors, the dilatancy angle is at least 20° less than the friction angle.

Generally, it has been very common in soil and rock mechanics that the dilatancy angle is associated to the friction angle. Dealing with dilatancy angle relatively to the friction angle may be more realistic to be considered, for the granular soils and (hard) rocks. One of the first approaches regarding the relation between the dilatancy angle and friction angle was suggested by Taylor (1948). Basically, this author proposed that the angle of internal friction, in spite of its name, does not depend solely on internal friction since a portion of the shearing stress on a plane of failure is utilized to overcome interlocking. Thence, it was concluded that:

$$\tan\varphi = \tan\varphi_{\mathrm{cv}} + \tan\Psi \tag{3}$$

where φ_{cv} is a constant which is referred to the friction angle at constant volume, i.e., no dilation is occurred. The relation of these two parameters may be also expressed by Eq. 4 following the sawtooth model (Houlsby 1991).

$$\varphi = \varphi_{\mathrm{cv}} + \Psi \tag{4}$$

That is indeed similar to the previous relation in stating that friction angle term is equal to the sum of a constant and the term of dilatancy. Within this approach, the changing process of dilatancy angle is induced by the variations in friction angle. Therefore, the dilatancy angle is considered to be a constant value if the friction angle is supposed to be so. Additionally, assuming a hardening procedure for friction angle of a rock (between an initial and a final value) in the course of loading (e.g., see Eq. 12), dilatancy angle follows implicitly the same procedure of change. In fact, dilatancy angle term, as the difference between a constant (φ_{cv}) and the term of friction angle is limited to a constant value when the friction angle gets to its final value during its hardening process. As a result of this dependency, the dilatancy angle may return to being constant unrealistically soon upon the definition of a quick hardening process for friction angle.

Furthermore, the use of a constant dilatancy angle value based on the rock mass quality was recommended by Hoek and Brown (1997). These authors then suggested the value of $\Psi = \varphi/4$ for very good quality rock masses, $\Psi = \varphi/8$ for average quality rock masses, $\Psi = 0$ for very poor quality rock masses.

Considering the dilatancy angle as a constant value in many numerical studies may be ascribed to trivial knowledge that is generally realized about how the dilatation of a rock changes, specially in the post-peak regime (or, post-failure regime). However, this assumption is not physically realistic, according to the primary study of Detournay (1986). This author proposed a relationship between the dilatancy of a rock and the plastic shear strain. As a common example of the problems encountered by consideration of a constant dilatancy, it was shown that simulation of tunnel closure in a rock is unrealistic using a constant dilatancy since there is no bound on the volume increase that the material can experience. The solution proposed in the latter reference was defining a tangent dilatancy factor K_p^* that decays from an initial value K_p (which is a function of the friction angle so that $K_p = (1 + \sin\varphi)/(1 - \sin\varphi)$) according to an exponential function of the plastic shear strain γ, such that:

$$K_p^* = 1 + (K_p - 1)\exp\left(-\frac{\gamma}{\gamma^*}\right) \tag{5}$$

where γ^* can most usefully be related to the maximum inelastic volume increase Δ^* as:

$$\gamma^* = \frac{\Delta^*}{\ln\frac{(K_p + 1)}{2}} \tag{6}$$

This proposition seems to be limited to the definition of a (positive) value for dilatancy which could decay until a (possible) residual value of 1. Another proposition was made recently by El Moustapha (2014) which suggests similarly a decay from a defined initial value of dilatancy angle to a final value as a function of plastic shear strain. This type of change in dilatancy factor is for instance the case for a dilatant behavior which is tended to degrade (a less dilatant response), like what could be observed in the course of a tunnel closure. Although, it may not cover all possible variety of a rock response throughout the evolution of plastic shear strain. For instance, given the gradual response of a rock during a large-scale deep excavation, propagation of the fractures and creation of the localized shear bands may primarily induce a dilatancy tendency in the rock within the fractured zone. This likely tendency is not supposed to remain constant afterward consisting in a limited dilatant volumetric response of the material in that zone. This behavior could be *a priori* modeled through an increase in the dilatation parameter (due to fractures opening/macro-crack propagation and creation of localization of deformation in the planar bands) and an ultimate reduction process after the peak of deviatoric stress (possible closure or no more opening mode of the fractures/no more development of the shear bands). The aforesaid type of change in dilatancy angle (with respect to the literature) seems to be inadequate to simulate this two-steps volumetric behavior of a rock. Therefore, a better numerical solution which can describe a more sophisticated dilatation behavior of a rock is desirable, as it is intended to be addressed in this study.

3 Numerical Framework

The numerical framework used in this study is presented in this section consisting in the basic elasto-plastic constitutive law and our development for considering the variable dilatancy angle, on one hand. The corresponding field equations, implemented in the finite element code LAGAMINE—developed at Université de Liège (Charlier 1987; Collin 2003)—consider a deformable two-phase medium: solid and water. On the other hand, with regard to numerical analysis of strain localization in the course of an underground excavation, the application addressed in this paper, the classic finite element method suffers from a pathological sensitivity to the mesh size (Collin et al. 2009; Salehnia 2015). Hence, an enhanced approach is needed in order to properly model the localization process and post-localization behavior. In this sense, the second gradient formulation, as the used enhanced method, is also described in the following.

3.1 Classical Constitutive Law

A non-associated frictional elasto-plastic model integrating with a Drucker–Prager yield surface (Drucker and Prager

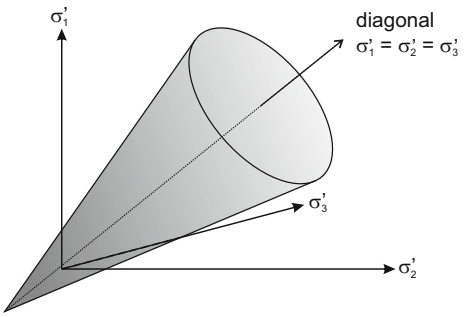

Fig. 1 Representation of the Drucker–Prager yield surface in the principle effective stress space

1952) (Fig. 1) is used in this study as the classical constitutive law. The yield limit taking into account the compressive stress to be negative reads:

$$F \equiv II_{\hat{\sigma}} + m\left(I_\sigma - \frac{3c}{\tan\varphi_c}\right) = 0 \tag{7}$$

where I_σ is the first stress invariant (Eq. 8), $II_{\hat{\sigma}}$ is the second deviatoric stress invariant (Eq. 9) where $\hat{\sigma}_{ij}$ is the deviatoric stress tensor, c is the cohesion, φ_c is the compression friction angle, and the parameter m is defined by Eq. 10.

$$I_\sigma = \sigma_{ij}\delta_{ij} \tag{8}$$

$$II_{\hat{\sigma}} \equiv \sqrt{\frac{1}{2}\hat{\sigma}_{ij}\hat{\sigma}_{ij}}; \quad \text{where } \hat{\sigma}_{ij} = \sigma_{ij} - \frac{I_\sigma}{3}\delta_{ij}, \tag{9}$$

$$m = \frac{2\sin\varphi_c}{\sqrt{3}(3-\sin\varphi_c)} \tag{10}$$

In addition, Terzaghi's postulate is assumed to define the effective stress tensor σ'_{ij}, which engenders the deformation of solid skeleton, relatively to total stress tensor σ_{ij} and the pore water pressure field p_w:

$$\sigma'_{ij} = \sigma_{ij} + p_w\delta_{ij} \tag{11}$$

where δ_{ij} is the Kronecker symbol.

Moreover, hardening and/or softening of friction angle and/or cohesion are allowed within this model through the hyperbolic functions (Barnichon 1998), such that:

$$\varphi_c = \varphi_{c0} + \frac{(\varphi_{cf} - \varphi_{c0})\varepsilon^p_{eq}}{B_\varphi + \varepsilon^p_{eq}} \tag{12}$$

$$c = c_0 + \frac{(c_f - c_0)\varepsilon^p_{eq}}{B_c + \varepsilon^p_{eq}} \tag{13}$$

where φ_{c0} and φ_{cf} are the initial and final compression friction angles, c_0 and c_f are the initial and final cohesions, and B_φ/B_c are the values of equivalent plastic strain for which half of hardening/softening on friction angle and/or cohesion is achieved (see Fig. 2). In addition, ε^p_{eq}, the equivalent plastic strain, with regard to which the variations in friction angle and cohesion are defined, is given by:

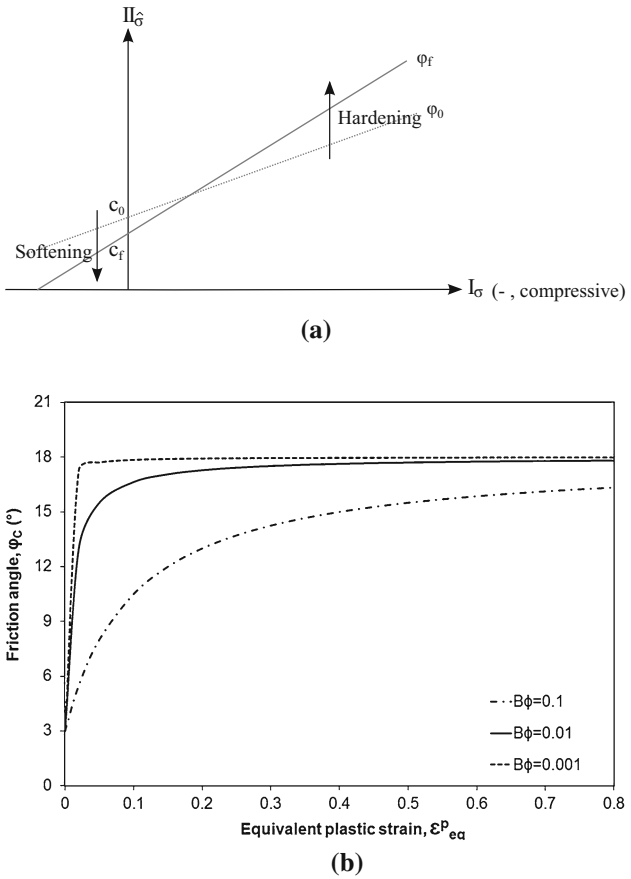

Fig. 2 **a** Schematic representation of the yield limit, in the $(I_\sigma, II_{\hat{\sigma}})$ plane, under φ_c hardening and c softening. **b** Hardening of friction angle from the initial value of $\varphi_{c0} = 3°$ to the final value of $\varphi_{cf} = 18°$, for three values of B_φ

$$\varepsilon^p_{eq} = \int_0^t \sqrt{\frac{2}{3}\left(\dot{\varepsilon}^p_{ij} - \frac{\dot{\varepsilon}^p_v}{3}\delta_{ij}\right)\left(\dot{\varepsilon}^p_{ij} - \frac{\dot{\varepsilon}^p_v}{3}\delta_{ij}\right)}\,dt \tag{14}$$

Furthermore, flow rule defines the increment of plastic strain in the material after it hits its yield limit, which is presented in a general form of:

$$\dot{\varepsilon}^p_{ij} = \dot{\lambda}\frac{\partial g}{\partial \sigma'_{ij}} \tag{15}$$

where $\dot{\lambda}$ is called plastic multiplier. $\partial g/\partial\sigma'_{ij}$ governs the direction of plastic strain increment where g is plastic potential function. Considering a non-associated plasticity, plastic potential surface is defined by Eq. 16 where the parameter m' is obtained through Eq. 17.

$$g \equiv II_{\hat{\sigma}} + m' I_\sigma = 0 \tag{16}$$

$$m' = \frac{2\sin\psi}{\sqrt{3}(3-\sin\psi)} \tag{17}$$

where ψ is the dilatancy angle. Thus, with application of the variable dilatancy angle (see Sect. 3.2), a modification of the potential surface can be then induced during the computation.

3.2 Proposed Formula for Considering the Variable Dilatancy Angle

To overcome difficulties associated to the application of a constant dilatancy angle—as described in Sect. 2—in our numerical analyses, a new formula is proposed. It defines the change in dilatancy angle in function of the equivalent plastic strain based on an introduced initial, peak, and limit value of dilatancy angle. With respect to the former studies (Barnichon 1998; El Moustapha 2014), the new formula has been developed in a semi-empirical manner with regard to a literature review of some various response of a rock—with special emphasis on Boom clay—evidenced through the triaxial tests and tunnel excavation observations. It has been implemented in the library of the finite element code LAGAMINE used in this study.

In fact, the new formula is aimed to address two main aspects lacked in most of the existing methods (e.g., see Eq. 5). First, it is intended to provide the possibility of simulating a two-steps and a transitional volumetric behavior by definition of three (instead of two) main factors of the dilatancy angle. Thence, for instance, a primary contracting behavior and subsequent dilatancy tendency of a material can be desirably reproduced. Alternatively, the likely tendency to dilatation of a rock within the opened fractures and the zone with localization of deformation created due to the tunneling, and a degradation of this tendency (Detournay 1986) because of the possible closure of the fractures/no more development of the localized bands could be numerically addressed (see Sect. 4). Therefore, besides that the dilatation behavior of a material could be simulated spatially differently (with regard to amount of computed plastic strain), it is varying in time following the loading procedure and the relative response of material. This aspect is in contrast with the unrealistic approach followed by consideration of a constant dilatancy angle.

Second, the three main parameters of the model (Ψ_{peak}, Ψ_{lim}, and Rat_Ψ in Eq. 18) are possible to be freely defined, and they can be positive or negative. Hence, for instance, an initial contraction (a negative initial value of dilatancy angle) and a subsequent dilatation could be reproducible.

Equation 18 presents the new proposition to vary the dilatancy angle:

$$\Psi = \frac{\Psi_{lim}}{2} + \left(\Psi_{peak} - \Psi_{lim}\right) + \frac{\left[\left(\Psi_{peak} \times Rat_\Psi\right) - \left(\Psi_{peak} - \Psi_{lim}\right)\right]\left[\varepsilon^p_{eq} - D_\Psi\right]}{B_\Psi + \left[\varepsilon^p_{eq} - D_\Psi\right]} \quad \left\{\text{for } \varepsilon^p_{eq} > D_\Psi\right\} \tag{18}$$

where Ψ_{peak} is the peak value of dilatancy angle, Ψ_{lim} is the limit value of the dilatancy angle that it cannot be outstepped, ε^p_{eq} is the equivalent plastic strain, B_Ψ is the value of equivalent plastic strain for which half of the change in dilatancy angle is achieved, and D_Ψ is the value of equivalent plastic strain beyond which the dilatancy angle varies, with respect to Eq. 18. A nonzero D_Ψ could then induce a delay in this variation process. Before the condition $\varepsilon^p_{eq} > D_\Psi$ is satisfied, dilatancy angle takes a constant value indicating its initial value, such that:

$$\Psi = \Psi_{peak} \times Rat_\Psi, \quad \text{where } Rat_\Psi \neq 0 \quad \left\{\text{for } \varepsilon^p_{eq} \leq D_\Psi\right\} \tag{19}$$

In addition, the parameter Rat_Ψ is defined as the ratio between the peak of dilatancy angle and its initial value. Then, it can make distinguishable the initial value of the dilatancy angle from its peak value. In fact, with regard to Eq. 19, the dilatancy angle is initially (i.e., under the condition of $\varepsilon^p_{eq} \leq D_\Psi$) equal to $\Psi_{peak} \times Rat_\Psi$ if we give a Rat_Ψ value to the model (i.e., $Rat_\Psi \neq 0$). Then, when the condition $\varepsilon^p_{eq} > D_\Psi$ is satisfied, the dilatancy angle firstly evolves quickly to its peak value and then changes approaching its limit value, with respect to Eq. 18.

Through introduction of Rat_Ψ parameter, the possibility of modeling of a two-steps volumetric behavior could be realized. For instance, a dilatant behavior with an initial dilatancy value that is increased to a peak value, and it is then reduced toward a limit value; e.g., due to the opening of a fractures's network and a later consolidation phase. Figure 3 shows a schematic example of the variations of dilatancy angle through definition of Rat_Ψ parameter. It is recalled that there is no restriction in definition of "positive" or "negative" values for the three main factors of dilatancy angle (i.e., Ψ_{peak}, Ψ_{lim}, and Rat_Ψ). Indeed, these values could be calibrated with respect to the loading procedure and the corresponding material behavior.

It must be noted that the dilatancy angle obtained by Eq. 18 is subsequently checked with regard to the condition

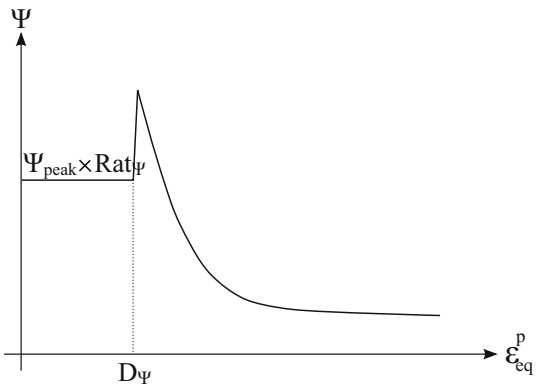

Fig. 3 A schematic example of the variation process of dilatancy angle

20. The latter is aimed to ensure that the obtained Ψ would not have gone beyond the defined limit value during its process of change.

$$\text{if } |\Psi_{\text{peak}} - \Psi| > |\Psi_{\text{peak}} - \Psi_{\text{lim}}| \Rightarrow \Psi = \Psi_{\text{lim}} \tag{20}$$

3.3 Theoretical Approach for Modeling of Strain Localization

Given the need to an enriched method for properly modeling of strain localization, the prediction of the material localization response is regularized in this study in the framework of microstructure continuum theory, using a second gradient continua. The local second gradient method, following the pioneering works of Mindlin (1964) and Germain (1973), is then applied in which the kinematics includes macrokinematics as well as microkinematics (Chambon et al. 1998, 2001). Hence, a microkinematic gradient field υ_{ij} is defined to describe strain and rotation at the microscale. Additional terms are then added to the classical continuum mechanics through the internal virtual work of a given body. Thus, for every kinematically admissible virtual displacement field $u_i^\star$ and virtual microkinematic gradient field $\upsilon_{ij}^\star$, Eq. 21 gives the internal virtual work in the weak form. Following the principle of virtual work, the latter should be then equal to the external virtual work, as given by Eq. 22.

$$\mathscr{W}_{\text{I}}^\star = \int_\Omega \left(\sigma_{ij} \frac{\partial u_i^\star}{\partial x_j} + \tau_{ij} \left(\upsilon_{ij}^\star - F_{ij}^\star \right) + \Sigma_{ijk} h_{ijk}^\star \right) \mathrm{d}\Omega \tag{21}$$

$$\mathscr{W}_{\text{E}}^\star = \int_{\Gamma_\sigma} \left(\overline{t}_i u_i^\star + \overline{T}_i \mathrm{D} u_i^\star \right) \mathrm{d}\Gamma \tag{22}$$

where Ω is the current solid configuration (volume), $u_i^\star$ is the virtual displacement field, τ_{ij} is the microstress tensor which is defined here in addition to the classical macrostress σ_{ij} and it is associated to the microstructures, $F_{ij}^\star = \partial u_i^\star / \partial x_j$ is the virtual macrodeformation gradient, and Σ_{ijk} is the double stress, dual of the virtual (micro) second gradient $h_{ijk}^\star$ $(=\partial \upsilon_{ij}^\star / \partial x_k)$. The latter needs an additional constitutive law and it is defined within an elastic law (Mindlin 1964) as a function of (micro) second gradient of the virtual displacement. This second gradient law depends on one elastic parameter D to which the shear band's width is proportional (Chambon et al. 1998). With regard to Eq. 22, $\overline{T}_i$ is an external (double) force per unit area in addition to $\overline{t}_i$ as the external (classical) traction forces per unit area, and the both are applied on the part Γ_σ of the boundary of Ω. $\mathrm{D}u_i^\star$ is the normal derivative of $u_i^\star$.

Moreover, within the framework of a coupled hydro-mechanical analysis, the above local second gradient formulation is accomplished giving the mass balance expression for the fluid (water) phase as Eq. 23, for every kinematically admissibles virtual pore water pressure field $p_{\text{w}}^\star$ (Collin et al. 2006). In this extension, it has been assumed that the fluid has no influence at the microstructure level, and the double stress Σ_{ijk} has then no link with the pore water pressure.

$$\int_\Omega \left(\dot{S} p_{\text{w}}^\star - m_i \frac{\partial p_{\text{w}}^\star}{\partial x_i} \right) \mathrm{d}\Omega = \int_\Omega Q p_{\text{w}}^\star \mathrm{d}\Omega - \int_{\Gamma_q} \overline{q} p_{\text{w}}^\star \mathrm{d}\Gamma \tag{23}$$

where $\dot{S}$ is the time derivative of the water mass inside Ω, m_i is the water mass flow (see Eq. 24), Q is a sink term, and $\overline{q}$ is the input water mass per unit area prescribed on the boundary portion Γ_q.

The water motion is governed by the general Darcy's law with regard to which, the water mass flow is given by:

$$m_i = -\rho_{\text{w}} \frac{k_{\text{w}}}{\mu_{\text{w}}} \left(\frac{\partial p_{\text{w}}}{\partial x_j} \right) \tag{24}$$

where k_{w} is the intrinsic water permeability, and μ_{w} is the water dynamic viscosity.

Furthermore, it is assumed that microkinematic gradient is equal to the macrodeformation gradient, i.e., $\upsilon_{ij} = F_{ij}$, and thence, the virtual microkinematic gradient is also equal to the virtual macrodeformation gradient $(\upsilon_{ij}^\star = F_{ij}^\star)$. These assumptions are then introduced through a field of Lagrange multipliers λ_{ij} (Chambon et al. 1998). Hence, the governing equations 21, 22 of the local second gradient model within the framework of principle of virtual work read:

$$\begin{aligned} &\int_\Omega \left(\sigma_{ij} \frac{\partial u_i^\star}{\partial x_j} + \Sigma_{ijk} \frac{\partial \upsilon_{ij}^\star}{\partial x_k} \right) \mathrm{d}\Omega \\ &- \int_\Omega \lambda_{ij} \left(\frac{\partial u_i^\star}{\partial x_j} - \upsilon_{ij}^\star \right) \mathrm{d}\Omega = \int_{\Gamma_\sigma} \left(\overline{t}_i u_i^\star + \overline{T}_i \upsilon_{ik}^\star n_k \right) \mathrm{d}\Gamma \end{aligned} \tag{25}$$

$$\int_\Omega \lambda_{ij}^\star \left(\frac{\partial u_i}{\partial x_j} - \upsilon_{ij} \right) \mathrm{d}\Omega = 0 \tag{26}$$

where n_k is the normal vector to the boundary portion Γ_σ.

Equations 25, 26 and 23 are held for any time t and the virtual quantities in these equations are dependent on the time t.

4 On Application of the Model to a Gallery Excavation

The numerical simulation of a deep gallery excavation, focusing on the strain localization development around the opening, is presented in this section. It aims to illustrate the influence of using the variable dilatancy angle, through the new proposition, while dealing with one practical problem in rock engineering. In fact, in the course of a large-scale

tunneling, the material could be largely deformed and fractured, and its real behavior may not be realistically addresses through the use of a constant dilatancy angle. In this sense, a correct estimation of the dilatancy variations could be of particular importance.

4.1 Definition of the Model

A gallery excavation in Boom clay host rock is modeled in the plane strain state taking into account the initial stress anisotropy. The initial stresses as well as the initial pore water pressure are applied with respect to the corresponding in-situ values at the level of HADES URL (Mol, Belgium), such that: $\sigma_{yy} = 4.5$ MPa, $\sigma_{xx} = 3.8475$ MPa (i.e., an earth pressure's coefficient at rest of $K_0 = 0.855$), and $p_w = 2.25$ MPa. The two-dimensional mesh geometry and boundary conditions of the model are schematically shown in Fig. 4. It consists in a quarter of the gallery, with a total excavated radius of 1.25 m, modeled assuming symmetry along x- and y-axes. The model is discretized with a total number of 9455 nodes and 2370 elements which are become finer by getting closer to the gallery wall. To correctly establish the symmetry along x- and y-axes, the normal displacements and water flow in addition to the normal derivatives of displacements are restricted along the symmetry axes. The latter kinematic boundary condition consists in $\partial u_x/\partial y = \upsilon_{12} = 0$ along the x axis and $\partial u_y/\partial x = \upsilon_{21} = 0$ along the y axis, i.e., symmetry of the radial displacements (u_r) around the symmetric boundaries (Zervos et al. 2001).

Moreover, the aforesaid initial stresses and pore water pressure are considered to be released on the gallery wall to the atmospheric pressure of 100 kPa during an excavation period of 1 day. In fact, this progressive release is intended for an implicit consideration of 3D impact of excavation front in its proximity through our 2D simulation.

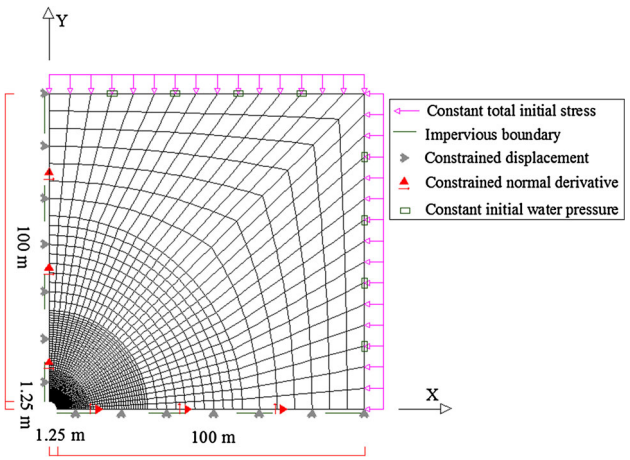

Fig. 4 The mesh geometry and boundary conditions of the model

In the course of a large-scale excavation, the likely fractures opening and macro-cracking are expected based on the in-situ observations. This phenomenon could realistically result in a dilatant behavior of the material (e.g., see Houlsby 1991; Kirkebø 1994). In the similar manner, brittle dilatant deformation accompanied by the fracture porosity have been extensively observed in Boom formation at the HADES URL, according to Dehandschutter et al. (2004). The shear induced fractures have been in fact evidenced during the tunneling in Boom clay (Mertens et al. 2004). In addition, this type of fracturing is often preceded by development of the localization of strains in narrow so-called shear bands, as it is focused in our modeling. All together, we propose to analyze the fractures development and the relative dilatancy tendency of the rock in the course of a gallery excavation through numerical simulation of strain localization in shear band mode around the opening using our variable dilatancy formula. To clarify the need to consider a variable dilatancy throughout the tunneling simulation, three computations is performed: one using a constant moderate Ψ equal to 5°, one using a null dilatancy angle, and the other one with application of variable Ψ, as described in the next section.

Tables 1 and 2 list the hydro-mechanical parameters used in our modelings. Apart from the dilatancy factors, the mechanical parameters given in Table 1 consist of a constant set of basic parameters of the model for Boom clay, chosen with respect to the former studies and numerical calibrations (Bernier et al. 2007b; Salehnia 2015). The final cohesion c_f, which controls the cohesion softening in the elasto-plastic behavior state, is chosen to be 30 kPa based on our former parametric studies (Salehnia et al. 2013a, b). In fact, considering the cohesion softening, as shown in the latter references, has an important role in initialization of strain localization during a numerical simulation. Material softening can be considered as the macroscopic reflection of inhomogeneities at the microscopic scale (micro-cracks, fractures, etc.). Furthermore, the second gradient elastic parameter (D) is introduced for our numerical analysis of strain localization with respect to the description given in Sect. 3.3. This modulus to which the shear band's width is proportional is chosen equal to 2000 N based on the latter references.

4.2 Discussion on the Results

The results of three simulations are presented in Figs. 5 and 6 in terms of increment of deviatoric strain and total deviatoric strain, respectively. The contours of increment of deviatoric strain could demonstrate the evolutionary creation and activity of the shear bands with localization of strain in different time steps. The ultimate extension of this

Table 1 Mechanical parameters defined for the modelings

Parameter	Symbol	Value			Unit
		$\Psi = 5°$	$\Psi = 0°$	Variable Ψ	
Young elastic modulus	E	300	300	300	MPa
Poisson ratio	ϑ	0.125	0.125	0.125	–
Specific mass of the grains	ρ_s	2700	2700	2700	kg/m^3
Initial compression friction angle	φ_{c0}	8	8	8	°
Final compression friction angle	φ_{cf}	18	18	18	°
Hardening coefficient	B_φ	0.01	0.01	0.01	–
Initial cohesion	c_0	300	300	300	kPa
Final cohesion	c_f	30	30	30	kPa
Softening coefficient	B_c	0.01	0.01	0.01	–
Second gradient elastic modulus	D	2000	2000	2000	N
Dilatancy angle	Ψ	**5**	**0**		°
Peak of dilatancy angle	Ψ_{peak}			**8**	°
Limit of dilatancy angle	Ψ_{lim}			**−1.5**	°
Dilatancy ratio	Rat_Ψ			**−0.06**	–
Dilatancy coefficient	B_Ψ			**0.001**	–
Dilatancy coefficient	D_Ψ			**0.017**	–

Bold values indicate the corresponding dilatancy factors defined in different simulations

Table 2 Hydraulic parameters defined for the modelings

Parameter	Symbol	Value	Unit
Specific mass of water	ρ_w	1×10^3	kg/m^3
Porosity	n	0.39	–
Water permeability	k	3×10^{-19}	m^2
Water compressibility	$\frac{1}{\chi_w}$	5×10^{-10}	Pa^{-1}
Water dynamic viscosity	μ_w	1×10^{-3}	Pa s

zone where the localized shear bands are created can signify the damaged zone caused by excavation. Additionally, the contours of total deviatoric strain visualize the synthesis of the whole history of the shear bands' activity in the accumulated time.

Firstly, with regard to the simulation with constant dilatancy angle, $\Psi = 5°$, it is observed in Fig. 5a that considering a constant value of Ψ did not allow the appearance of strain localization. In fact, introducing of a constant (nonzero) dilatancy angle into the model could be somehow interpreted as definition of a highly enough dilatant material for which there is a resistance to plastic shearing (Kirkebø 1994) and to the localization (Bernier et al. 2007a) associated to the possible pore pressure drop. In this sense, in the hydraulic point of view, due to principally the existence of a constant (positive) dilatancy angle, besides the influence of the own excavation and decompression process, the pore water pressure is considerably decreased overall in the vicinity of the gallery (see Fig. 7a) resulting in an increase in the effective stress. Accordingly, the corresponding result, in terms of total deviatoric strain, in Fig. 6a consists in no created localized shear bands throughout the simulation. Therefore, dilatation, mainly due to its coupling with pore water pressure, could provide a resistance to localization in spite of the impact of the defined cohesion softening to trigger the strain localization.

Second, taking into account of a null dilatancy angle, the results of simulation of the gallery excavation are shown in Figs. 5b and 6b. With respect to Fig. 5b, it is observed that some localized bands could be created and there is some activity of the bands during the simulation. However, these bands seem not be well-constructed in the vicinity of the gallery wall. This issue can be more obviously perceived by Fig. 6b. Looking at the whole problem in an hydraulic point of view, some decrease in the pore water pressure within a zone around the gallery is still expected due to the decompression, regardless of the defined null dilatancy angle parameter (see Fig. 7b). This can impose some resistance to the development of bands of localization (one may also see Bernier et al. 2007a; Salehnia 2015). Consequently , these bands are not properly formed very close to the gallery wall (e.g., see the contour of 1 day in Fig. 6b). The encountered decrease pattern (local drainage) of pore water pressure within the whole gallery's vicinity is shown in Fig. 7b, which is in fact quite comparable with the result of application of a constant Ψ in Fig. 7a. Thence, the coupled hydro-mechanical process seems to limit (or delay) a correct physical regularization of the localized shear bands, even though the localization has occurred.

On the other hand, with respect to the literature and site observation, as mentioned beforehand in Sect. 4.1, a

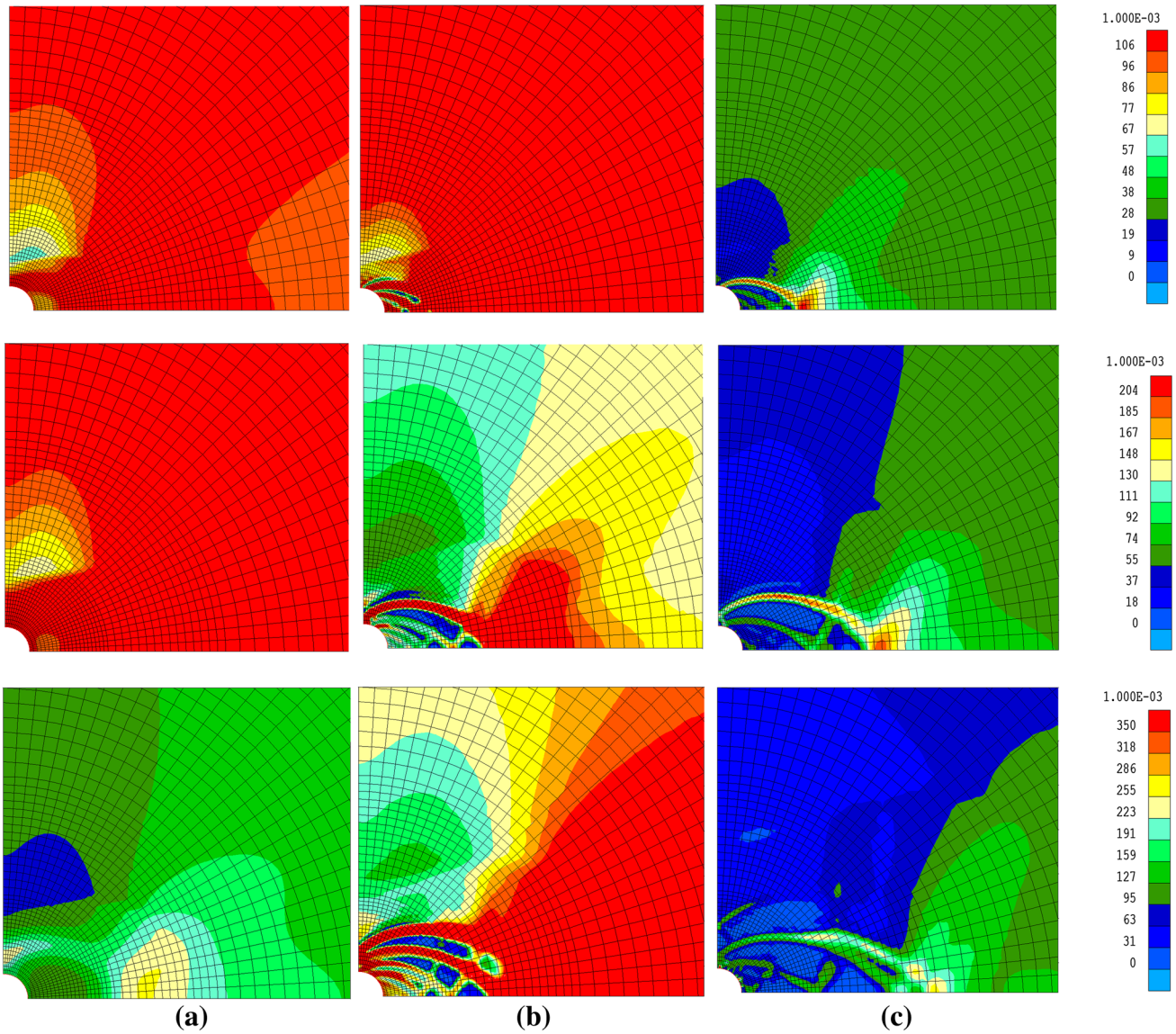

Fig. 5 Increment of deviatoric strain after 0.65 day (*top row*), 0.85 day (*middle row*), and 1 day (*bottom row*) for the simulation with: **a** $\Psi = 5°$. **b** $\Psi = 0°$. **c** Variable Ψ

dilatant behavior of the rock could be considered realistic as a primary phenomenon upon fracturing due to excavation. This response is not supposed to be constant, though. Therefore, through the third computation, we propose that the simulation of strain localization development around the gallery is integrated with an evolution of the dilatancy angle to a peak value (maximum dilatation tendency) coinciding with the creation of the localized shear bands during the excavation. This maximum dilatancy tendency may then lie in the fractures opening/macro-crack propagation in the course of a real excavation.

Subsequently, this peak of dilatancy is declined consisting in a less (positive) or negative dilatation tendency of the rock. This latter decline of dilatancy is basically consistent with the pioneering work of Detournay (1986) indicating that there must be a bound on the dilatation that the material experience during the excavation. This author then suggested a decay form an initial dilatancy value as described in Sect. 2. The non-constant dilatancy tendency of a rock upon tunneling has been similarly addressed in some other studies with regard to the literature (e.g., Kirkebø 1994; Alejano and Alonso 2005).

Thence, considering the definition of an initial value of dilatancy angle (through the Rat_{Ψ} parameter; Eq. 19), this initial value is evolved to a peak positive value of 8° that is chosen within the range proposed by Bernier et al. (2007b) (see Table 1). This evolution occurs in parallel with the creation of shear bands with localization of deformation (once $\varepsilon^{p}_{eq} > D_{\Psi}$; one may see Eqs. 18 and 19). This dilatancy tendency is then declined with reference to a chosen

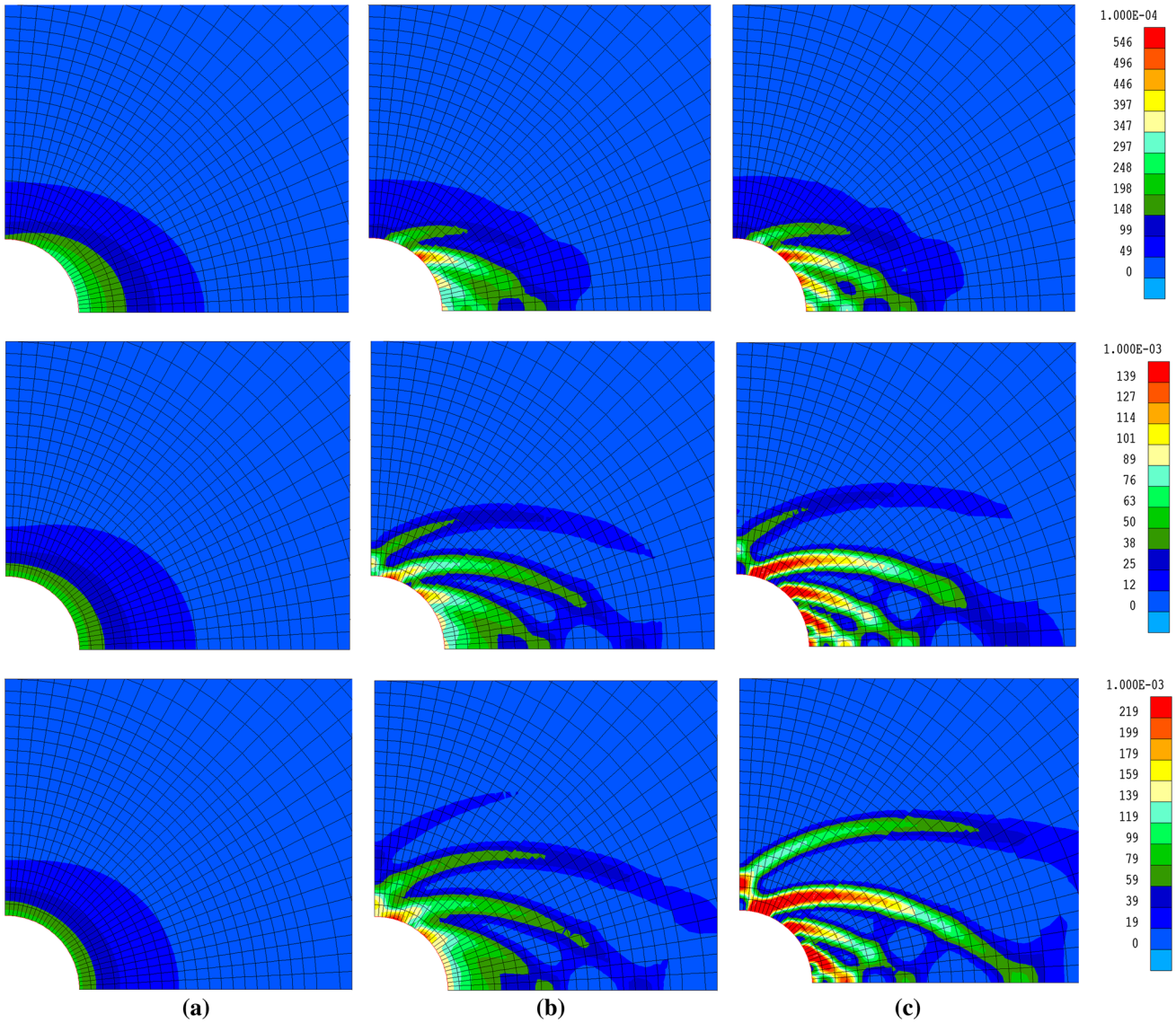

Fig. 6 Total deviatoric strain after 0.65 day (*top row*), 0.85 day (*middle row*), and 1 day (*bottom row*) for the simulation with: **a** $\Psi = 5^\circ$. **b** $\Psi = 0^\circ$. **c** Variable Ψ

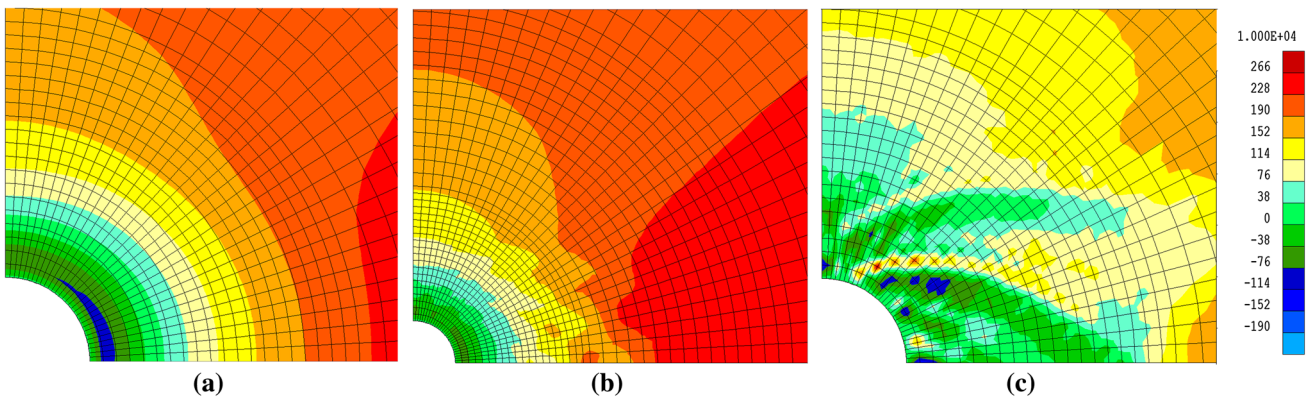

Fig. 7 Contour of pore water pressure after 1 day for the simulation with: **a** $\Psi = 5^\circ$. **b** $\Psi = 0^\circ$. **c** Variable Ψ

low negative limit value. The process of decline is followed with respect to the purely numerical parameters B_Ψ and D_Ψ, and in function of the equivalent plastic strain (see Eq. 18). Dealing with a large strain problem, D_Ψ is chosen relatively high making a retardation in the variation process of dilatancy angle following its peak value. Moreover, a low value of B_Ψ could desirably help to accelerate the decline process of dilatancy angle (see Sect. 3.2). The numerical parameter B_Ψ indeed affect the rate of the change, similarly to the role of B_φ and B_c in the hardening and softening processes of friction angle and cohesion (Eqs. 12, 13). The latter acceleration is aimed to prevent a remained high enough dilatancy angle in the course of excavation which might result in the likely resistance to localization, as it has been already discussed.

In overall, while the peak and limit values of dilatancy angles could determine the variation range of dilatancy angle, the three other parameters could influence the variation procedure of dilatancy angle after its peak. In this sense, it must be noted that the parameter Rat_Ψ does not only signify the initial statue of Ψ. In addition, it has also an implicit impact on the subsequent variation process of dilatancy angle, with respect to the third term in Eq. 18.

It must be noted that the objective of this latter modeling is limited to illustration of the influence of application of variable dilatancy angle, with a realistic estimation of the corresponding parameters, in contrast with a constant value while dealing with the fractures and strain localization simulation in the course of a large-scale excavation. However, the studied galley is only an academic case for which we do have no quantification of the real volumetric response due to fractures propagation.

The results of the last simulation with variable Ψ are demonstrated in Figs. 5c and 6c. Comparing these results with the corresponding results of the two other simulations in Fig. 5 and more obviously in Fig. 6, it is observed that the simulation with variable Ψ results in the clearer and better constructed localized shear bands. In fact, within the localized zone close to the gallery wall, these bands could be individually appeared accompanied by an instantaneous dilatation tendency imposed within them (with respect to the accumulated plastic strain in the relative zone; see Eq. 18) while the same process does not occur between these bands. The maximum dilatation tendency indeed lies within the appearance/onset of the localized shear bands (in our simulation) or the likely fractures opening in the course of a real excavation. Consequently, well-formed shear bands are reproduced in the vicinity of the gallery. This phenomena might then imply that the encountered fracturing/onset of localized shear bands is responsible for the major dilatancy evolution, in the microscopic point

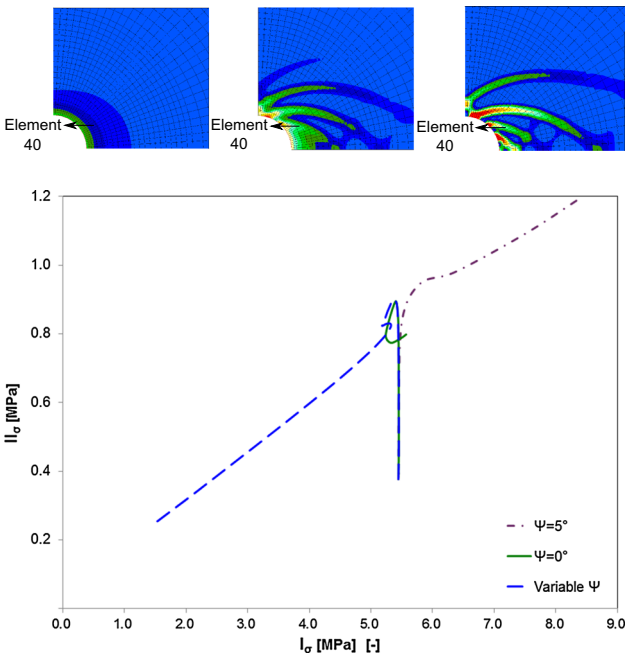

Fig. 8 Effective stress path of the element 40 in the $(I_\sigma, II_{\hat{\sigma}})$ plane for the simulations with $\Psi = 5°$, $\Psi = 0°$, and variable Ψ. The element position is demonstrated in the top image on the contour of total deviatoric strain after 1 day in each case

of view. The latter could be then considered besides our basic analysis of shear banding in the scale of gallery, i.e., macroscopic scale.

In the hydraulic point of view, the aforementioned peak of dilatation tendency results in the decrease in pore pressure in the course of excavation and by the onset of the bands while this dilatation is then followed by a diminishing trend (see Fig. 9). This pattern of non-constant decreasing Ψ thus controls the dilatation behavior of the rock. In the first place, there is not such constant reduction tendency of pore pressure close to the gallery wall, which would impose a resistance to the correct development of the localized shear bands. In the second place, following the dilatancy change during the excavation time passing its maximum value, there is some generation of the pore water pressure, and more importantly within the bands, while the redistribution of the pore pressure around the gallery throughout the decompression process is spatially variable (see Fig. 7c). This hydraulic behavior could consequently help the physical regularization of the shear bands with finite thickness—similarly to the concept presented in Thakur (2011)—in addition to the role of strain softening in initiation of the shear strain localization.

Furthermore, the effective stress path for a random element 40 within the created localized zone is demonstrated in Fig. 8 for the last simulation as well as two previous simulations with constant ψ. The localization solution is accompanied by a reduced shear stress and the

material's resistance. This behavior consists in a dominant decrease in the first stress invariant with the decrease in second invariant of deviatoric stress beyond its maximal value along the stress path of the studied element, with regard to the simulation with variable ψ. On the contrary, the non-localized solution corresponding to the application of $\Psi = 5^\circ$ is illustrated through its opposite-ward stress path consisting in an increase in the deviatoric stress, with an increased first stress invariant. This has been integrated with the overall decrease in pore water pressure in the vicinity of the gallery, in an hydraulic point of view (see Fig. 7a). Concerning the case with application of a null dilatancy angle, a slight increase in the first stress invariant toward the end of the excavation period is observed subsequently to some relative decrease. This phenomenon lies in the coupled response of the rock with respect to the encountered decrease pattern (local drainage) of pore water pressure within the whole gallery's proximity, as a result of decompression (see Fig. 7b).

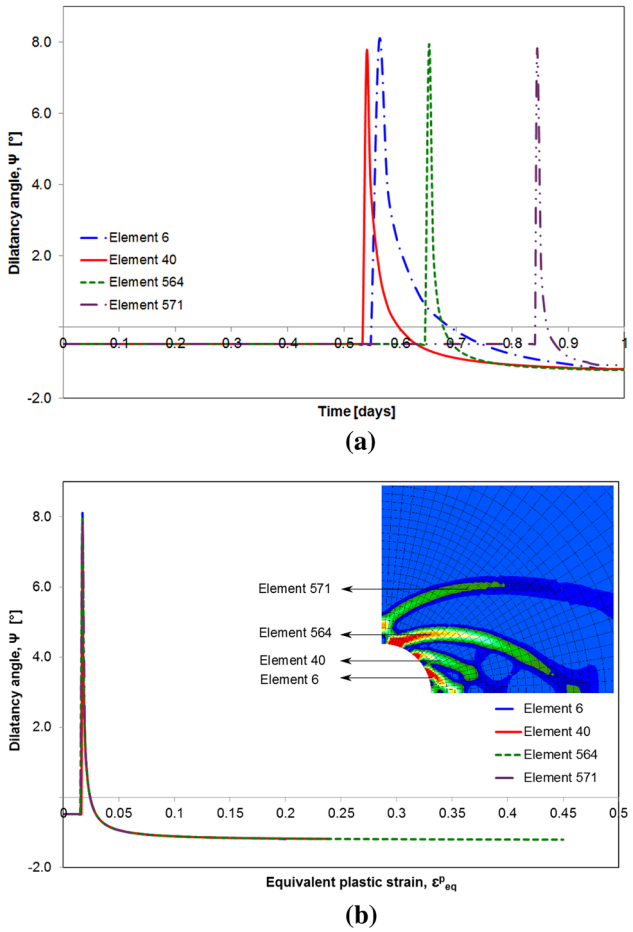

Fig. 9 The change of dilatancy angle in the course of excavation for the elements 6, 40, 564, and 571 within the localized zone around the gallery. **a** Dilatancy angle in function of the time. **b** Dilatancy angle in function of the equivalent plastic strain

Given the simulation with variable Ψ, Fig. 9 shows the variation of dilatancy angle for four random elements within the created localized bands. This variation is demonstrated in function of the time throughout the excavation (see Fig. 9a), and also in function of the equivalent plastic strain (see Fig. 9b). With respect to the evolutionary process of strain localization and the creation of the shear bands in time (see Fig. 5c), dilatancy angle varies in each element as observed in Fig. 9a. The peak of dilatancy angle for each element then coincides with the appearance of its corresponding band. With regard to a real gallery excavation, the latter may be then interpreted as the maximum dilatation of the rock taken place simultaneously with the fractures opening. Although, this dilatant behavior is not supposed to remain constantly within the fractured zone afterward. In addition, Fig. 9b shows that Ψ is changed for all the elements after attaining the equivalent plastic strain equal to the defined D_Ψ (=0.17).

5 Conclusions

A new formula for considering the variable dilatancy angle was presented in this paper. This proposition has been in fact motivated by the inconveniences associated to using a constant dilatancy angle in many numerical analyses dealing with the rock engineering problems. The proposed approach has been implemented in a finite element code integrating with an elasto-plastic hardening/softening model. It can be simply implemented in any numerical tool in rock mechanics field, in conjunction with the standard numerical models.

Within the framework of our new formula, three main factors of dilatancy angle are considered for a material consisting in an initial value, a peak value and a limit value, among which the dilatancy angle varies with respect to the plastic strain in the course of a loading process. As a result, a variety of volumetric responses can be realistically reproduced. A dilatant or contracting volumetric behavior of a rock as well as a dilatant/contracting transitional response can be in fact simulated based on the defined model's elements.

The new proposition has been applied to simulate a deep gallery excavation and the resulted strain localization development within the surrounding host rock. The studied material is Boom clay, the reference potential host rock for deep disposal of high-level nuclear waste in Belgium. The dilatancy tendency following the appearance of the localized shear bands (or, the propagation of fractures), due to the excavation, in the proximity of the opening could be realistically reproduced. Following the variation of dilatancy angle, this tendency is not remained constant spatially and in time afterward. The resulting hydro-

mechanical response of the rock around the gallery has been demonstrated that could prompt a well-formed development of the localized shear bands in the vicinity of the gallery. The corresponding results then challenged the use of a constant (positive/null) dilatancy angle throughout the simulation. In this sense, it has been shown that considering a constant (nonzero) dilatancy angle (during the excavation period) could impose a resistance to localization and shearing, despite that the cohesion softening has been taken into account in order to trigger the strain localization.

Acknowledgements The financial support of ONDRAF/NIRAS (Belgian National Agency for Radioactive Waste and enriched Fissile Material), and the fruitful cooperation of EURIDICE (European Underground Research Infrastructure for Disposal of nuclear waste in Clay Environment) are gratefully acknowledged. This work is part of the first author's Ph.D. thesis.

References

Alejano L, Alonso E (2005) Considerations of the dilatancy angle in rocks and rock masses. Int J Rock Mech Min Sci 42(4):481–507

Barnichon J-D (1998) Finite element modelling in structural and petroleum geology. PhD thesis, Université de Liège

Bastiaens W, Bernier F, Buyens M, Demarche M, Li XL, Linotte JM, Verstricht J (2003) The Connecting gallery. Technical report, EURIDICE. Report to European Commission

Bernier F, Li X, Bastiaens W, Ortiz L, Van Geet M, Wouters L, Frieg B, Blümling P, Desrues J, Viaggiani G et al (2007a) Fractures and self-healing within the excavation disturbed zone in clays (selfrac). Final report to EC (Project FIKW-CT2001-00182). EUR, 22585

Bernier F, Li XL, Bastiaens W (2007b) Twenty-five years' geotechnical observation and testing in the tertiary Boom clay formation. Géotechnique 57(2):229–237

Bésuelle P, Viggiani G, Desrues J, Coll C, Charrier P (2014) A laboratory experimental study of the hydromechanical behavior of Boom clay. Rock Mech Rock Eng 47(1):143–155

Blümling P, Bernier F, Lebon P, Martin CD (2007) The excavation damaged zone in clay formations time-dependent behaviour and influence on performance assessment. Phys Chem Earth A B C 32(8):588–599

Chambon R, Caillerie D, El Hassan N (1998) One-dimensional localisation studied with a second grade model. Eur J Mech A Solids 17(4):637–656

Chambon R, Caillerie D, Matsuchima T (2001) Plastic continuum with microstructure, local second gradient theories for geomaterials: localization studies. Int J Solids Struct 38(46):8503–8527

Chapman N, Hooper A (2012) The disposal of radioactive wastes underground. Proc Geol Assoc 123(1):46–63

Charlier R (1987) Approche unifiée de quelques problèmes non linéaires de mécanique des milieux continus par la méthode des éléments fini. PhD thesis, Université de Liège

Charlier R, Collin F, Pardoen B, Salehnia F (2015) Numerical modelling of shear banding around openings in clayey rocks. Application to URL dedicated to nuclear waste disposals. In: International symposium on energy geotechnics (1st.: 2015: Barcelona). Universitat Politècnica de Catalunya. Departament d'Enginyeria del Terreny, Cartogràfica i Geofísica

Coll C (2005) Endommagement des roches argileuses et perméabilité induite au voisinage d'ouvrages souterrains. PhD thesis, Université Joseph-Fourier-Grenoble I

Collin F (2003) Couplages thermo-hydro-mécaniques dans les sols et les roches tendres partiellement saturés. PhD thesis, Université de Liège

Collin F, Chambon R, Charlier R (2006) A finite element method for poro mechanical modelling of geotechnical problems using local second gradient models. Int J Numer Methods Eng 65(11):1749–1772

Collin F, Levasseur S, Chambon R (2009) Numerical post failure methods in multiphysical problems. Eur J Environ Civ Eng 13(7–8):983–1004

Dehandschutter B, Vandycke S, Sintubin M, Vandenberghe N, Gaviglio P, Sizun J-P, Wouters L (2004) Microfabric of fractured Boom clay at depth: a case study of brittle-ductile transitional clay behaviour. Appl Clay Sci 26(1):389–401

Detournay E (1986) Elastoplastic model of a deep tunnel for a rock with variable dilatancy. Rock Mech Rock Eng 19(2):99–108

Drucker DC, Prager W (1952) Soil mechanics and plastic analysis or limit design. Q Appl Math 10(2):157–165

El Moustapha K (2014) Identification of an enriched constitutive law for geomaterials in the presence of a strain localisation. PhD thesis, Université de Grenoble

Germain P (1973) The method of virtual power in continuum mechanics. Part 2: Microstructure. SIAM J Appl Math 25(3):556–575

Hoek E, Brown E (1997) Practical estimates of rock mass strength. Int J Rock Mech Min Sci 34(8):1165–1186

Houlsby G (1991) How the dilatancy of soils affects their behaviour. University of Oxford, Department of Engineering Science

Kirkebø S (1994) A numerical study of excavations in low permeable soils. University of Trondheim, Norwegian Institute of Technology

Mertens J, Bastiaens W, Dehandschutter B (2004) Characterisation of induced discontinuities in the boom clay around the underground excavations (URF, Mol, Belgium). Appl Clay Sci 26(1):413–428

Mindlin R (1964) Micro-structure in linear elasticity. Arch Ration Mech Anal 16(1):51–78

ONDRAF/NIRAS (2001) Technical overview of the safir 2 report: safety assessment and feasibility interim report 2. Technical report NIROND 2001–05 E

Papamichos E (2010) Borehole failure analysis in a sandstone under anisotropic stresses. Int J Numer Anal Methods Geomech 34(6):581–603

Papanastasiou PC, Vardoulakis IG (1992) Numerical treatment of progressive localization in relation to borehole stability. Int J Numer Anal Methods Geomech 16(6):389–424

Salehnia F, Charlier R, Levasseur S (2013a) Modeling of strain localization around the radioactive waste disposal galleries. In: Coupled phenomena in environmental geotechnics, CPEG 2013. CRC Press, pp 443–450

Salehnia F, Charlier R, Levasseur S (2013b) Numerical modelling of the excavated damaged zone in boom clay. In: International EAGE workshop on geomechanics and energy

Salehnia F, Charlier R, Sillen X, Dizier A (2015a) Modeling of excavation damaged zone through the strain localization approach in boom clay. In: Proceedings of the 14th international conference of International Association for Computer Methods and Recent Advances in Geomechanics, IACMAG 2014. CRC Press, pp 335–340

Salehnia F, Collin F, Li XL, Dizier A, Sillen X, Charlier R (2015b) Coupled modeling of excavation damaged zone in boom clay: strain localization in rock and distribution of contact pressure on the gallery's lining. Comput Geotech 69:396–410

Salehnia F (2015) From some obscurity to clarity in Boom clay behavior: analysis of its coupled hydro-mechanical response in the presence of strain localization. PhD thesis, Université de Liège

Taylor DW (1948) Fundamentals of soil mechanics. Soil Sci 66(2):161

Thakur V (2011) Numerically observed shear bands in soft sensitive clays. Geomech Geoeng Int J 6(2):131–146

Tsang C-F, Bernier F, Davies C (2005) Geohydromechanical processes in the excavation damaged zone in crystalline rock, rock salt, and indurated and plastic clays—in the context of radioactive waste disposal. Int J Rock Mech Min Sci 42(1):109–125

Vermeer PA, De Borst R (1984) Non-associated plasticity for soils, concrete and rock. HERON 29(3)

Zervos A, Papanastasiou P, Vardoulakis I (2001) Modelling of localisation and scale effect in thick-walled cylinders with gradient elastoplasticity. Int J Solids Struct 38(30):5081–5095

Zervos A, Vardoulakis I, Papanastasiou P (2007) Influence of nonassociativity on localization and failure in geomechanics based on gradient elastoplasticity. Int J Geomech 7(1):63–74